DISCLAIMER

Si / InGaN Core/Shell Hierarchical Nanowire Arrays and their Photoelectrochemical Properties

*Yun Jeong Hwang, Cheng Hao Wu, Chris Hahn, Hoon Eui Jeong, and Peidong Yang**

Department of Chemistry, University of California, Berkeley, California 94720, and Materials Sciences Division, Lawrence Berkeley National Laboratory, 1 Cyclotron Road, Berkeley California 94720

*Address correspondence to p_yang@berkeley.edu

Abstract

Three dimensional hierarchical nanostructures were synthesized by the halide chemical vapor deposition (HCVD) of InGaN nanowires on Si wire arrays. Single phase InGaN nanowires grew vertically on the sidewalls of Si wires and acted as a high surface area photoanode for solar water splitting. Electrochemical measurements showed that the photocurrent density with hierarchical Si/InGaN nanowire arrays increased by 5 times compared to the photocurrent density with InGaN nanowire arrays grown on planar Si (1.23 V vs RHE). High resolution transmission electron microscopy showed that InGaN nanowires are stable after 15 hours of illumination. These measurements show that Si/InGaN hierarchical nanostructures are a viable high surface area geometry for stable solar water splitting.

KEYWORDS: Hierarchical nanostructure, InGaN nanowire, Si wire, photoanode, solar water splitting

Introduction

Photolysis of water with semiconductor materials has been investigated as a clean and renewable energy conversion process by storing solar energy in chemical bonds such as hydrogen.[1-3] Since Fujishima and Honda[4] reported the capability of water splitting with TiO_2, metal oxide semiconductors have been studied extensively due to their stability under photo-anodic conditions.[5-6] However, the valence band of metal oxide semiconductors consists mainly of O 2p orbitals resulting in a low energy maximum (around +3 V vs NHE compared to +1.23 V vs NHE for the water oxidation reaction). This leads to a significant loss in energy from the large difference in potential between the valence band and water oxidation reaction. In addition, lowering the metal oxide bandgap energy for visible light absorption generally comes at the cost of moving the conduction band minimum (CBM) towards lower potentials than the hydrogen reduction potential which cannot perform spontaneous solar water splitting.

On the other hand, metal nitrides have less positive valence band maximum (VBM) potentials than metal oxides because N 2p orbitals have smaller ionization energies than O 2p orbitals.[6-7] For example, GaN is one of the nitride semiconductors that have been studied for photocatalytic applications[8-11] because its CBM and VBM straddle the hydrogen reduction (H^+/H_2) and water

oxidation (H_2O/O_2) potentials. Although GaN has a large bandgap (3.4 eV), indium alloying to form InGaN can tune the bandgap from the ultraviolet to the near infrared region[12] encompassing the entire solar spectrum. The $In_{0.5}Ga_{0.5}N$ alloy has a bandgap of around 2.0 eV which is desirable for overall water splitting considering the overpotential for the water oxidation reaction.[13-14] Moses et al.[15] calculated that the VBM of InGaN alloy increases in energy almost linearly with indium composition. Therefore, the InGaN alloy was suggested to accomplish spontaneous overall water splitting with up to 50% indium incorporation since both the CBM and VBM can satisfy the energetic requirements. Experimentally, single crystalline $In_xGa_{1-x}N$ nanowires with compositions up to x = 0.4~0.5 have been realized.[16] Although the InGaN alloy is a very promising water splitting material, only a few studies have been reported[17-19] with no studies on nanowire geometries.

One dimensional nanostructures have been demonstrated to be efficient in photoelectrochemical (PEC) cell and photovoltaic cell applications because they can decouple the directions of light absorption and charge carrier collection.[20-21] When the life time of the minority carrier is short, the minority carrier can recombine in bulk before it reaches the semiconductor/electrolyte junction. However, because nanowires have a small radius, the minority carrier can diffuse to the surface before recombination. This can increase charge separation efficiency, especially when the minority carrier diffusion length is comparable to the radius of the nanowire.

Here, we investigate the photoanodic properties of Si/InGaN hierarchical nanostructures consisting of InGaN nanowires grown directly on Si wire arrays. Compared with one dimensional nanostructures, this hierarchical nanostructure provides additional InGaN/electrolyte interfacial area. Complex two or three dimensional nanostructures such as interlinked branches[22-26] and dendritic[27] nanostructures have shown enhanced efficiencies for solar water splitting from increased charge transport or charge separation. In addition, the Si/InGaN hierarchical nanostructure arrays can potentially increase light absorption due to increased scattering from the hierarchical structures.

High surface area Si/InGaN hierarchical nanowire arrays were grown by conformal coating of InGaN nanowires on patterned Si wire arrays on n-Si (111) substrate (resistivity < 0.005 Ωcm). Using plasma-enhanced chemical vapor deposition (PECVD), a 200 nm silicon oxide layer was deposited on a n-Si(111) wafer and photo-lithographically patterned. The oxide layer was dry etched with CHF_3/CF_4 plasma and followed by evaporation of a 120 nm Au film and lift-off of the photoresist. The Si wire arrays were subsequently grown from the patterned Au catalysts with $SiCl_4$ (99.99% Sigma Aldrich) and 10% H_2/Ar at 875 °C. The Vapor-Liquid-Solid (VLS) grown Si wires were 750~ 800 nm in diameter and 20~25 μm in length. After Si wire growth, the Au catalyst was removed from the tops and sidewalls of the Si wires by KI/I_2 gold etchant.

For photoanodic applications, we have reported that a n/n heterojunction can produce higher photocatalytic activity from better charge separation.[28] Therefore, we chose to n-type dope the Si wire arrays with phosphorus since the as-grown InGaN nanowires are n-type. Post-growth doping of the Si wires could also create a better electron conducting pathway for charge collection. A n-type Si substrate, spin coated by spin-on-diffusant (P509, Filmtronics), was placed on top of a Si wire array with a 1 mm spacer and annealed at 900 °C for 4hrs with 10% O_2/Ar flow to diffuse vaporized phosphorus into silicon wire. Afterwards, Si wire arrays were

annealed at 1000 °C under vacuum with Ar flow for an additional 2hr. Under analogous conditions, a silicon (100 nm) on insulator substrate was measured to have a carrier concentration of 10^{20} cm^{-3} from its resistivity (four point).

Single-phase InGaN nanowires with homogeneous composition were grown on Si wire arrays and planar n-Si(111) in a three zone HCVD furnace as described in a previous report.[16] $GaCl_3$ (99.999% metals basis, Alfa Aesar), $InCl_3$ (99.999% metals basis, Alfa Aesar), and NH_3 were used as III/V precursors with N_2 as a carrier gas. The composition of InGaN nanowires was controlled by modifying the $GaCl_3$ and $InCl_3$ precursor temperatures. Immediately prior to InGaN nanowire growth, the native oxide was removed from Si wires by using a buffered HF solution. Samples were placed on the 30^o tilted quartz plate for conformal coating of the Si wire arrays. During the reaction, the $GaCl_3$ and $InCl_3$ precursors were kept at 70 °C and 390-415 °C respectively.

Scanning electronic microscopy (SEM) images of hierarchical Si/InGaN nanowire arrays show that InGaN nanowires (less than 100 nm in diameter) grow conformally on the Si wire arrays (Figure 1). The cross sectional SEM image (Fig. 1d) of a hierarchical Si/InGaN nanowire clearly shows six facets of the Si wire, usually observed in VLS grown Si wires with the <111> growth direction, with InGaN nanowires grown vertically out of the Si facets. The conformal InGaN coating over Si wires can prohibit photooxidation of Si from direct contact between Si and the electrolyte. Similarly, InGaN nanowires grew vertically from the planar Si(111) substrate as shown in top down and cross sectional SEM images (Fig. 1e-f). Elemental analysis using SEM energy-dispersive x-ray spectroscopy (EDS) showed that $In_xGa_{1-x}N$ nanowires have a composition of x = 0.08~0.1.

X-ray diffraction (XRD) patterns for vertically grown InGaN nanowires on planar Si(111) show predominantly the wurtzite 002 peak (Figure 2) which is consistent with previous reports of epitaxially grown InGaN nanowires on Al_2O_3(001) and quartz[16]. However, Si/InGaN hierarchical nanowire arrays show a decrease in intensity of the 002 peak while the 100 and 101 peaks get stronger compared to InGaN nanowires on planar Si. This can be attributed to the difference in geometric orientation of InGaN nanowires on Si wires vs planar Si.

To measure the PEC properties of Si/InGaN, electrodes were constructed from the as grown samples. An In-Ga eutectic was applied to the back side of the Si substrate and a copper wire was connected with silver paste. The substrate and wire were subsequently covered with insulating epoxy (Hysol) to expose only the desired surface area. Samples were immersed in a pH 3 H_2SO_4 solution with 0.5 M of Na_2SO_4 salt as an electrolyte. All PEC measurements were conducted at pH 3 since photoanodic etching of GaN has been observed in both strongly basic (1M KOH) and strongly acidic (1M H_2SO_4) electrolyte.[29] Working electrodes were illuminated through a quartz window of a PEC glass cell. A 300 W Xe lamp (Newport, 6258) was coupled with a diffuser for uniform illumination intensity (samples typically 0.3~0.5 cm^2) and an AM 1.5 filter (Newport, 81094) for simulated sunlight. The illumination intensity was measured with a calibrated Si photodiode. Photocurrents were measured in a three-electrode configuration using an Ag/AgCl reference electrode and a Pt mesh counter electrode.

Figure 3a shows dark current and photocurrent densities plotted vs the reversible hydrogen electrode (RHE) for Si/InGaN hierarchical nanowire arrays and InGaN nanowires grown on the planar Si substrate. The dark current densities of both samples were negligible until 1.5 V vs RHE. The photocurrent density for hierarchical nanowire arrays increased beginning from 0.1 V vs RHE and reaches 33 $\mu A/cm^2$ at 1.23 V vs RHE while InGaN nanowire arrays grown on planar Si only reached a current density of 6 $\mu A/cm^2$ at the same bias. We believe that the higher surface areas of hierarchical nanostructures result in higher photocurrent by enhancing the optical pathway and assisting in charge separation.

Hierarchical nanowire arrays were further tested under different illumination conditions (Fig. 3b) to determine whether the measured photocurrent was due to light absorption. As the input light intensity increases, the InGaN nanowires should absorb more photons resulting in higher photocurrent at the same bias voltage. The photocurrent density increased from 16 $\mu A/cm^2$ to 33 $\mu A/cm^2$ (at 1.23 V vs RHE) when the portion of UV increased by removing the AM 1.5 filter. It increased further to 62.6 $\mu A/cm^2$ (at 1.23 V vs RHE) under a higher light intensity of 350mW/cm^2 without the AM 1.5 filter.

One of the concerns for metal nitride semiconductors is chemical stability to anodic photooxidation. To test the stability of InGaN nanowires, we illuminated the nanowires with a high light intensity (350 mW/cm^2) for 15 hrs in pH 3 electrolyte. The photocurrent density was stable and did not change before and after illumination. Also, no noticeable decomposition of InGaN nanowires was observed by SEM and XRD after illumination. Figures 4a and b show high resolution TEM (HRTEM) images of InGaN nanowires taken from Si/InGaN hierarchical wire arrays after 15 hrs of illumination. The images clearly show that the crystalline structure of InGaN nanowires remains intact and with no observed structural decomposition or surface oxide formation. The surface of InGaN nanowires was clean indicating that they were not oxidized during the measurement.

To examine the performance of Si/InGaN photoanodes we can compare the measured photocurrent with the theoretical maximum photocurrent assuming a quantum efficiency (QE) of 1. The bandgap of $In_{0.1}Ga_{0.9}N$ is 3.1 eV which can have maximum photocurrent of 1.31 mA/cm^2 for water splitting under AM1.5 illumination. However, the measured photocurrent is only 1.2% of this maximum photocurrent. Some important processes that can influence the QE in this system are light absorption, charge transport across the Si/InGaN junction, and charge separation at the semiconductor/electrolyte junction. InGaN nanowires have a high absorption coefficient even on planar substrates.[16] Moreover, scattering within the Si/InGaN hierarchical structures is expected to increase light absorption. Therefore, light absorption is unlikely to be limiting the QE of Si/InGaN hierarchical structures. The charge transport between planar n-Si and InGaN nanowires was checked by measuring the I-V characteristics of the junction (Figure S1). These results suggest that charge transport across the Si/InGaN junction is also not a limiting factor. However, the shapes of the photocurrent curves are similar to materials known to have fast charge recombination and highly resistive charge transfer processes into solution. Therefore, we expect that a higher photocurrent can be achieved by improving the efficiency of the charge transport within InGaN nanowires and charge transfer at the semiconductor/electrolyte interface.

Several intrinsic material properties can influence excited carrier dynamics at the semiconductor/electrolyte junction. One property is the band bending (photovoltage) at this interface. III-nitrides have been reported to have varying degrees of Fermi level pinning depending on the growth method.[30-31] A direct result of this high electronic state density at the surface is a reduction in photovoltage at the semiconductor/electrolyte junction.[32] This is unfavorable since band bending is the driving force for the separation of photogenerated carriers. One possible method for decreasing surface states is to passivate the surface effectively. Another potential issue for solar water splitting with III-nitrides is fast carrier recombination. Fluorescence dynamics studies on InGaN and other highly strained III-nitride alloys have shown lifetimes on the order of sub 1 ns due to charge localization and native defects.[33-34] Therefore, these alloys tend to have short minority carrier diffusion lengths (<200 nm) which can prevent efficient charge transfer. We propose that the addition of an oxidation co-catalyst to the surface of our InGaN nanowires could significantly improve charge separation[35] during that short time-scale. An oxidation co-catalyst could also increase photocatalytic activity by reducing the required overpotential for water oxidation. Finally, studies have shown that the photocurrent of n-GaN electrodes is strongly correlated to its carrier concentration.[36] According to the charge transfer model at the semiconductor/electrolyte interface, the photocurrent decreases above the optimized carrier concentration due to the fast recombination in the space charge region. Photovoltage studies on our HCVD grown InGaN nanowires indicate that they are n-type from unintentional doping during growth. Therefore, we believe that the photocurrent can be optimized through better synthetic control of the doping concentration/mobility in InGaN nanowires.

In conclusion, we have demonstrated the potential for solar water splitting with high surface area Si/InGaN hierarchical nanowire arrays. An enhancement of 5 times in photocurrent was observed when the surface area increased from InGaN nanowires on planar Si to InGaN nanowires on Si wires. The photocurrent generated from Si/InGaN was constant over extended illumination times and no degradation of InGaN nanowires was observed by TEM. These measurements indicate that Si/InGaN hierarchical arrays can be used as stable photoanodes and are promising for efficient solar water splitting. Further work will be done to improve the performance of Si/InGaN hierarchical arrays by examining the effects of surface passivation, oxidation co-catalysts, and controlled doping on InGaN nanowires. Also, we plan to further increase visible light absorption by incorporating more indium into Si/InGaN hierarchical nanowire arrays.

Acknowledgements

This work was supported by the Director, Office of Science, Office of Basic Energy Sciences, Materials Sciences and Engineering Division, of the U.S. Department of Energy under Contract No. DE-AC02-05CH11231.

Supporting Information is available free of charge via the Internet at http://pubs.acs.org

References

1. Walter, M. G.; Warren, E. L.; Mckone, J. R.; Boettcher, S.W.; Santori, E. A.; Lewis, N. S. *Chem. Rev.* **2010,** *110,* 6446–6473.
2. Grätzel, M. *Nature* **2001**, 414, 338-344.
3. Maeda, K.; Domen, K. *J. Phys. Chem. Lett.* **2010**, 1, 2655-2661.
4. Fukishima, A.; Honda, K. *Nature* **1972**, 238, 37-38.
5. Rajeshwar, K. *J Appl Electrochem* **2007**, 37, 765-787.
6. Maeda, K.; Domen, K. *MRS Bulletin* **2011**, 36, 25-31.
7. Maeda, K.; Domen, K. *J. Phys. Chem. C.* **2007**, 111, 7851-7861.
8. Beach, J. D.; Collins, R. T.; Turner, J. A. *J. Electrochem. Soc.* **2003**, 150, A899-A904
9. Maeda, K.; Teramura, K.; Saito, N.; Inoue, Y.; Domen, K. *Bull. Chem. Soc. Jpnt.* **2007**, 80 , 1004-1010.
10. Wang, D.; Pierre, A.; Kibria, M. G.; Cui, K.; Han, X.; Bevan, K. H.; Guo, H.; Paradis, S. ; Hakima, A. R.; Mi, Z. *Nano. Lett.* **2011**, 11 , 2353-2357.
11. Jung, H. S.; Hong, Y. J.; Li, Y.; Cho, J. ; Kim, Y. J.; Yi, G. C. *ACS Nano*, **2008**, 2, 637-642.
12. Kuykendall, T.; Ulrich, P.; Aloni, S.; Yang, P. *Nat. Mater.* **2007**, *6* , 951-956.
13. Bolton, J. R.; Strickler, S. J.; Connolly, J. S. *Nature* **1985**, 316, 495-500.

14. Wang, H.; Deutsch, T.; Turner, J. A. *ECS Transactions* **2008**, 6, 37-44.

15. Moses, P. G.; Van de Walle. C. G. *Appl. Phys. Lett.* **2010, 9**6, 021908.

16. Hahn, C.; Zhang, Z.; Fu, A.; Wu, C. H.; Hwang, Y. J.; Gargas, D. J.; Yang, P. *ACS Nano*, **2011**, 5, 3970-3976.

17. Fujii, K.; Kusakabe, K.; Ohkawa, K.; *Jpn. J. Appl. Phys.* **2005,** 44, 7433–7435

18. Li, J.; Lin, J. Y.; Jiang, H. X.; *Appl. Phys. Lett.* **2008, 9**3, 162107.

19. Theuwis, A.; Strubbe, K.; Depestel, L. M.; Gomes, W. P. *J. Electrochem. Soc.* **2002**, 149, E173-E178.

20. Shankar, K.; Basham, J. I.; Allam, N. K.; Varghese, O. K.; Mor, G. K.; Feng. X.; Paulose, M.; Seabold, J. A.; Choi, K. S.; Grimes. C. A. *J. Phys. Chem. C.* **2009**, 113, 6327-6359.

21. Kayes, B. M.; Atwater, H. A.; Lewis, N. S. *J. Appl. Phys.* **2005**, *97*, 114302.

22. Lin, Y.; Zhou, S.; Liu, X.; Sheehan, S.; Wang, D. *J. Am. Chem. Soc.* **2009**, 131, 2772-2773.

23. Lin, Y.; Yuan, G.; Liu, R.; Zhou, S.; Sheehan, S. W.; Wang, D. *Chem. Phys. Lett.* **2011**, 507, 209-215.

24. Shi, J.; Hara, Y.; Sun, C.; Anderson, M. A.; Wang, X. *Nano. Lett.* **2011**, 11 , 3413-3419.

25. Cho, I. S.; Chen, Z.; Forman, A. J.; Kim, D. R.; Rao, P. M.; Jaramillo, T. F.; Zheng, X. *Nano. Lett.* **2011**, 11 , 4978–4984.

26. Bierman, M. J.; Jin, S. *Energy Environ. Sci.* **2009**, 2, 1050–1059.

27. Kay, A.; Cesar, I.; Grätzel, M. *J. Am. Chem. Soc.* **2006**, 128, 15714-15721.

28. Hwang, Y. J.; Boukai, A.; Yang, P. *Nano. Lett.* **2009**, 9 , 410-415.

29. Huygens, I. M.; Strubble, K.; Gomes, W. P. *J. Electrochem. Soc.* **2000**, 147, 1797-1802.

30. Kočan, M.; Rizzi, A.; Lüth, H.; Keller, S.; Mishra, U. K. *Phys. Stat. Sol. (b)* **2002**, 234, 773-777.

31. Segev, D.; Van De Walle, C. G. *Europhys. Lett.* **2006**, 76, 305-311.

32. Bard, A. J.; Bocarsly, A. B.; Fan, F. F.; Walton, E. G.; Wrighton, M. S. *J. Am. Chem. Soc.* **1980**, 102, 3671-3677.

33. Sun, C. K.; Keller, S.; Wang, G.; Minsky, M. S.; Bowers, J. E.; DenBaars, S. P. *Appl. Phys. Lett.* **1996**, 69, 1936-1938.

34. Chichibu, S.F.; Uedono, A.; Onuma, T.; Haskell, B.A.; Chakraborty, A.; Koyama, T.; Fini, P.T.; Keller, S.; Denbaars, S.P.; Speck, J.S.; Mishira, U.K.; Nakamura, S.; Yamaguchi, S.; Kamiyama, S.; Amano, H.; Akasaki, I.; Han, J.; Sota, T. *Nat. Mater.* **2006**, 5, 810-816.

35. Yoshida, M.; Yamakata, A.; Takanabe, K.; Kubota, J.; Osawa, M.; Domen, K. *J. Am. Chem. Soc.* **2009**, 131, 13218-13219.

36. Ono, M.; Fujii, K.; Ito, T.; Iwaki, Y.; Hirako, A.;Yao, T.; Ohkawa, K. *J. Chem. Phys.* **2007**, 126, 054708.

Figure Captions

Figure 1. Tilted (45°) SEM images of hierarchical Si/$In_xGa_{1-x}N$ nanowire arrays on Si (111) substrate with X = 0.08~ 0.1 (a-c). A fractured wire reveals the cross section (d) showing that InGaN nanowires grow vertically from the six Si wire facets. Top down (e) and cross sectional (f) SEM images of vertical $In_xGa_{1-x}N$ nanowires grown on a planar Si (111) substrate.

Figure 2. X-ray diffraction patterns of $In_xGa_{1-x}N$ nanowires (x = 0.08-0.10) grown on planar Si(111) (black) and Si wires (red). $In_xGa_{1-x}N$ nanowires grown on planar Si (111) show a higher intensity 002 wurtzite peak indicating mostly vertical growth of InGaN nanowires from the silicon surface (blue diamond for wurtzite peak of InGaN) . Hierarchical $Si/In_xGa_{1-x}N$ nanowire arrays show a 111 peak from Si (black dot) wires and all other wurtzite peaks.

Figure 3. Photoelectrochemical measurements on $Si/In_xGa_{1-x}N$ (x = 0.08~0.10) photoanodes. Photocurrent density plots (a) of hierarchical $Si/In_xGa_{1-x}N$ nanowire arrays (red) and planar $Si/In_xGa_{1-x}N$ (blue) under 100 mW/cm^2 without AM 1.5 filter show an increase in current for the hierarchical geometry. A representative dark current density plot is shown in black. Photocurrent density plots (b) of hierarchical $Si/In_xGa_{1-x}N$ nanowire arrays show a photocurrent dependence on illumination condition: red (100mW/cm^2, with AM 1.5 filter), blue (100mW/cm^2, without AM 1.5 filter), and green (350mW/cm^2, without AM 1.5 filter).

Figure 4. High resolution TEM images of a representative InGaN nanowire taken from hierarchical Si/InGaN nanowire arrays after 15 hours of illumination. Nanowires show no obvious photochemical etching or amorphous layer formation after illumination.

Figure 1

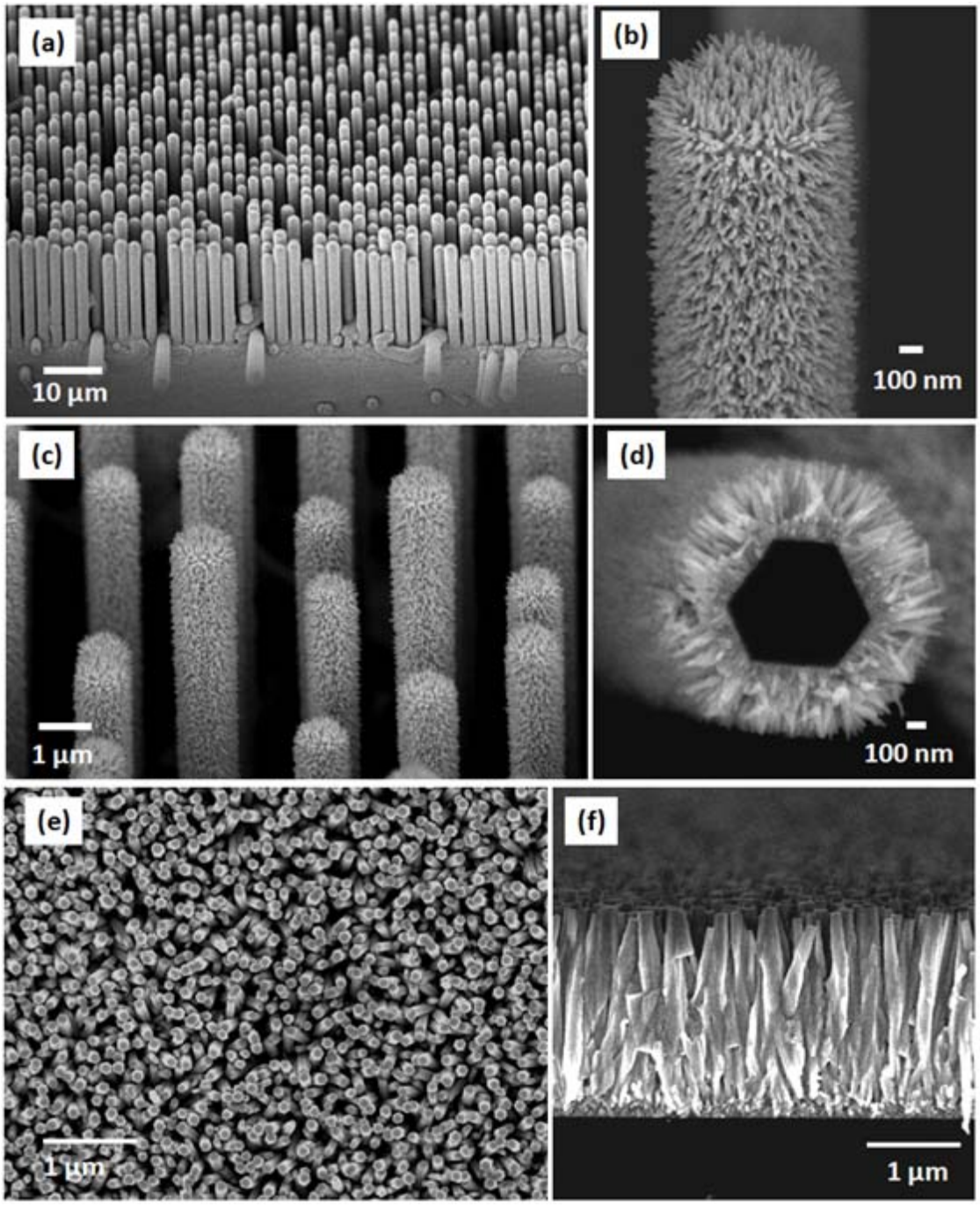

Figure 2

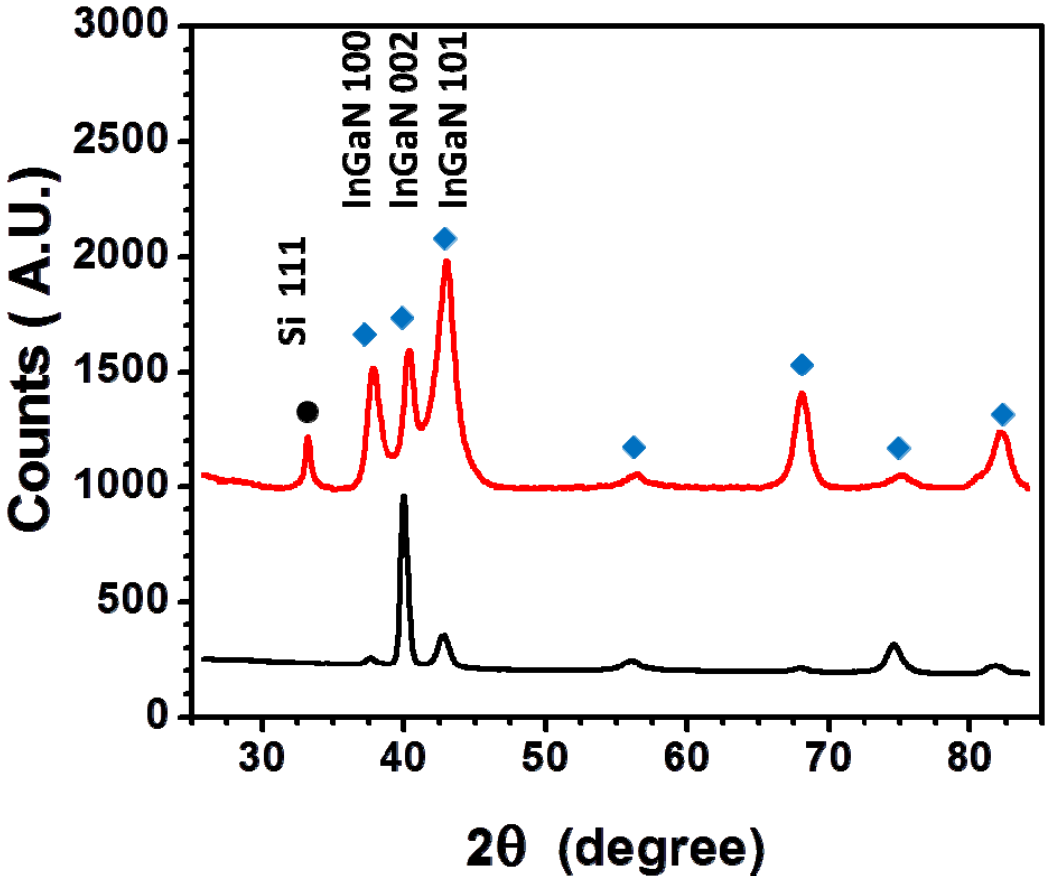
Counts (A.U.)
3000
2500
2000
1500
1000
500
0
30
40
50
60
70
80
2θ (degree)
Si 111
InGaN 100
InGaN 002
InGaN 101

Figure3

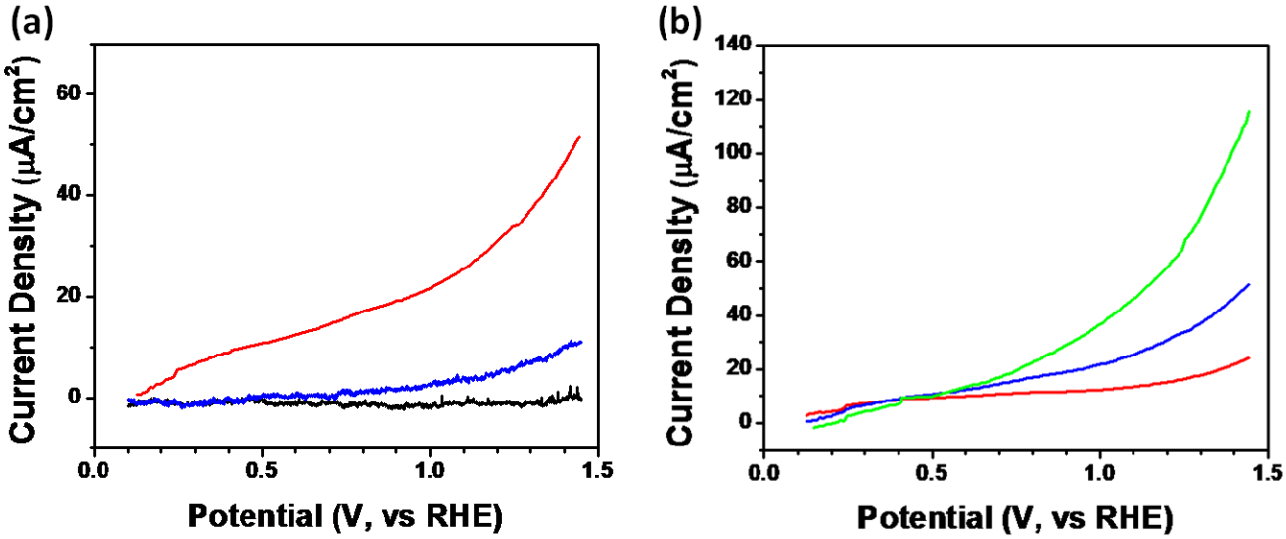

Figure 4

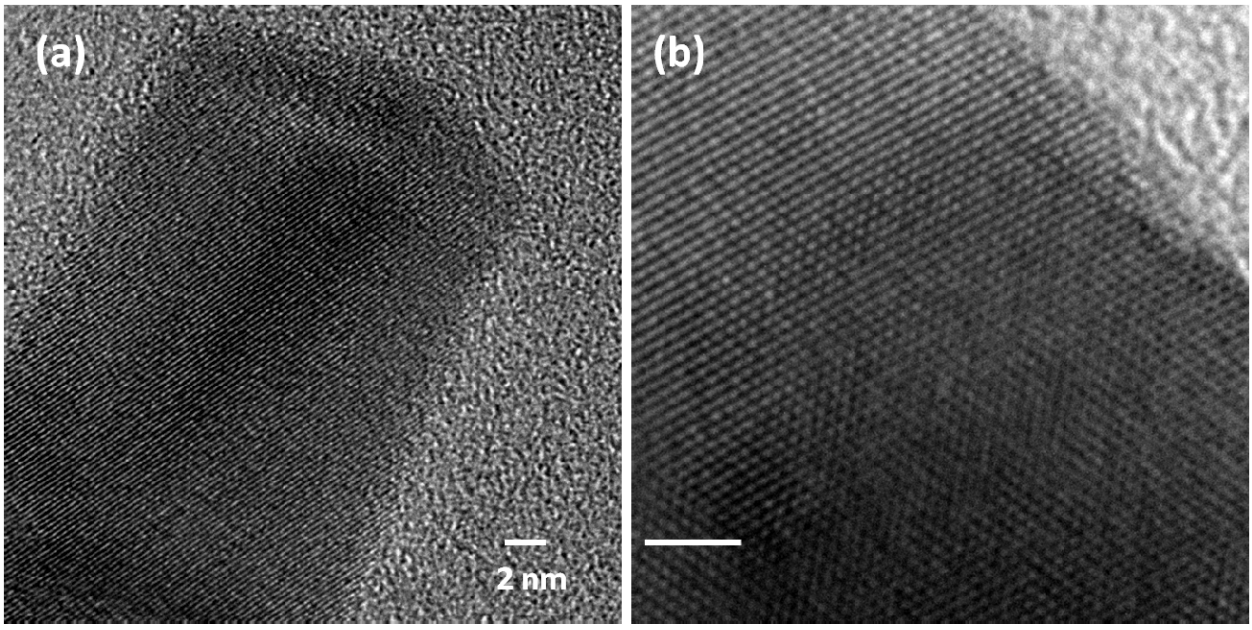

TOC

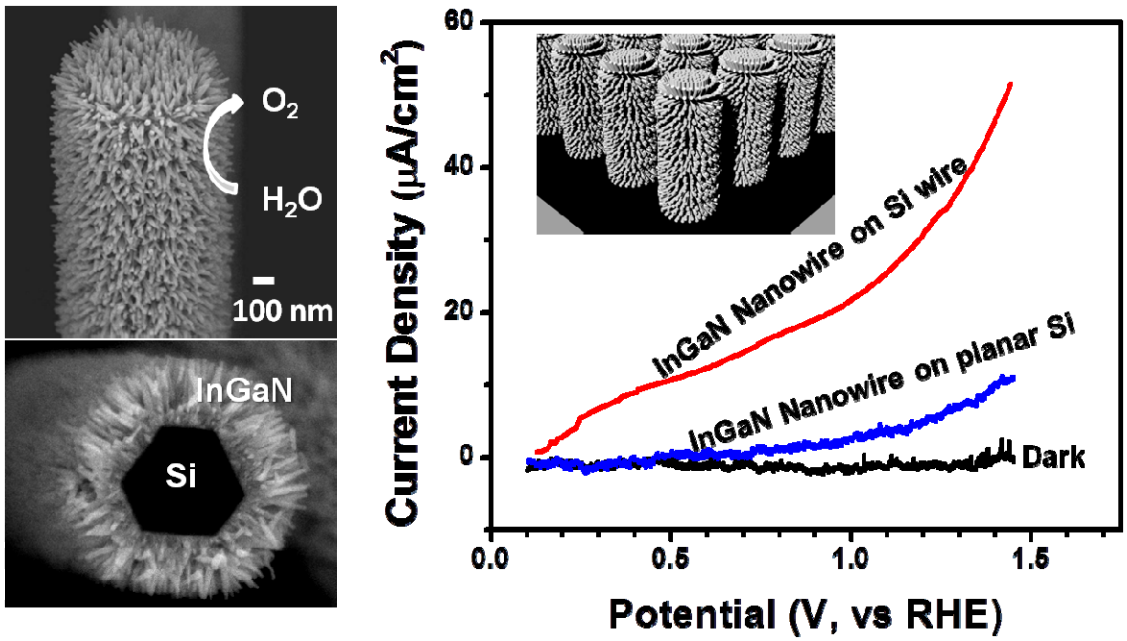
O2
H2O
100 nm
InGaN
Si
Current Density (μA/cm2)
60
40
20
0
0.0
0.5
1.0
1.5
Potential (V, vs RHE)
InGaN Nanowire on Si wire
InGaN Nanowire on planar Si
Dark

Acknowledgements: This work was supported by the Director, Office of Science, Office of Basic Energy Sciences, Material Sciences and Engineering Division, of the U.S. Department of Energy under Contract No. DE-AC02-05CH11231. We thank the National Center for Electron Microscopy for the use of their facilities.